JMATPRO	Journal of Advanced Materials and Processing 10 (1): 39-56, Winter 2022 http://jmatpro.iaun.ac.ir 20.1001.1.2322388.2022.10.1.4.7

Research Paper

Evolution of Biological Properties of Bioactive Diopside and Wollastonite for Bone Tissue Engineering

Ruhollah Zamani Foroushani[(1)], Ebrahim Karamian[(1)*], Mohammad Rafienia[(2)]

1. Advanced Materials Research Center, Department of Materials Engineering, Najafabad Branch, Islamic Azad University, Najafabad, Iran

2. Biomaterial, Nanotechnology and Tissue engineering Department of Advanced Medical Technology, Isfahan University of Medical Sci-ences, Isfahan, Iran

ARTICLE INFO

Article history:

Received 26 November 2021
Accepted 29 December 2021
Available online 1 January 2022

Keywords:
Bioactivity
Biomineralization
Cell responses
Diopside
Wollastonite

ABSTRACT

The present study aimed to synthesize and characterize diopside ($CaMgSi_2O_6$) and wollastonite ($CaSiO_3$) nano-bioceramics via a combination of mechano-chemical and calcination processes. In vitro biomineralization and cell responses of wollastonite and diopside were carried out using simulated body fluid (SBF) for up to 28 days and MG-63 osteoblast cells. Results revealed excellent tissue biomineralization of wollastonite and diopside through generating an apatite-like layer on the surface of nano-bioceramics. Wollastonite and diopside cell responses eventuated non-cytotoxicity by MG-63 osteoblast cells, and their viability and cell proliferation were verified. Results of alizarin red staining and alkaline phosphate enzyme of diopside and wollastonite evidenced great bioactivity and tissue biomineralization with respect to the release of Ca^{2+} and high absorption related to calcium activity, and high activity and growth of alkaline phosphate enzyme to repair bone tissue of diopside, and wollastonite was enhanced in contact with the MG-63 osteoblast cells. Regarding the addition of Mg^{2+} into the calcium-silicate network for the chemical stability network to improve biological properties, results of biological assays verified that diopside possessed high biological and cell responses in comparison to wollastonite; and both of them can be suggested as great bioactive and biocompatible candidates for biomedical applications.

Citation: Zamani Foroushani, R.; Karamian, E.; Rafienia, M. (2022) Evolution of Biological Properties of Bioactive Diopside and Wollastonite for Bone Tissue Engineering, Journal of Advanced Materials and Processing, 10 (1), 39-56. Dor: 20.1001.1.2322388.2022.10.1.4.7

* **Corresponding Author**
E-mail Address: karamian1970@gmail.com

1. Introduction

To restore bone defects is a significant challenge in medical and biomedical sciences, and finding alternative materials for bone tissues is vital. Calcium silicates ($CaSiO_3$ and Ca_2SiO_4) and calcium silicate-based ceramics have become the principal focus of biomaterials [1, 2]. The materials possess biological properties such as bioactivity and enhancement of cell interactions compared to traditional calcium phosphates like hydroxyapatite (HAp) or β–tricalcium phosphate [3]. Therefore, they are promising candidates as bone graft materials. Moreover, incorporating metal atoms (Mg, Zn, and Zr) into the crystalline structure of calcium silicates has improved their biological revenue [4-7]. In fact, silicate biomaterials, including wollastonite and Ca–Si–M ternary ceramics (M = Ti, Mg, Zn and Zr) are the topic of many research projects for bone tissue restoration usages. A significant feature of silicate biomaterials is their ability to release the silicon (Si) ion which persuades the growth and distinction of osteoblast cells to some extent [8-10]. Additionally, a precise study of $CaO–SiO_2$ ceramics showed their direct connection with bone. The study showed that ceramics including CaO and SiO_2 have suitable bioactivity and connection power to bone [9]. Recently, an extension of $CaO–SiO_2–MgO$ ceramics with diopside ($CaMgSi_2O_6$) topic has found special consideration in biomaterials applications, and diopside has currently been identified as a bioactive bioceramic. It was reported [10, 11] that the presence of magnesium (Mg) in the $CaO–SiO_2$ system by using diopside as a biomaterial. The chemical composition of diopside is similar to akermanite ($Ca_2MgSi_2O_7$). However, it possesses a lower degradability rate compared to akermanite and wollastonite. In addition, in the chemical composition of diopside, the calcium atom is replaced by a magnesium atom, and Mg–O bond is developed [11-13].

Since the Mg–O bonding energy is higher than that of the Ca–O bonding, the stability of the crystalline structure is increased [12]. On the other hand, the $CaO–SiO_2–MgO$ ceramic systems are appropriate for bone regeneration applications [13].

It was reported [14] that the mechanism of bioactivity of $CaO–SiO_2–MgO$ system ceramics is similar to silicate glass, which is related to the direct release of the Si ions. One of the significant bioceramic compounds is wollastonite ($CaSiO_3$), which has unique characteristics such as thermal stability and high hardness. Therefore, it has acquired abundant applications in the ceramic industry [15]. In addition, wollastonite possesses high bioactivity, so apatite layers appear on it and grow fast only after 3 days. Besides, the growth rate of the hydroxyapatite in nano-structured wollastonite was more than its growth rate in micro-structured wollastonite [16]. One of the most interesting synthesis processes of nano-structured bio-ceramics is mechano-chemical process. The particle sizes of nano-structured materials are less than 100 nm [17]. Due to their ideal physical and chemical properties, they attract much attention from scientific and research communities [18]. In the research, cell responses of MG-63 osteoblast cells, bio-mineralization, calcium activity, and alkaline phosphatase enzyme behavior on synthesized diopside ($CaMgSi_2O_6$) and wollastonite ($CaSiO_3$) nano-bioceramics via a combination of mechano-chemical and calcination processes were surveyed for biomedical applications.

2. Materials and methods

2.1. Raw materials

Calcium carbonate powder ($CaCO_3$) (Merck, Germany), silica (SiO_2) (Merck Co., Germany), and magnesium oxide (MgO) (Merck Co., Germany) were used to synthesize diopside and wollastonite compounds.

2.2. Synthesis of diopside and wollastonite

To synthesize diopside, 15.38 wt.% of MgO, 46.15%wt of SiO_2, and 38.46%wt of $CaCO_3$ were chosen, and then mechano-chemical process (ball milling) was carried out. In this process, ball–to–powder weight ratio and milling speed were 10:1 and 350 rpm, respectively, and the milling times were 5 min, 10 h and 20 h. Then, the developed powders were calcinated at 1200 °C for 2 h [19]. Similarly, the process was conducted to synthesize wollastonite, and the milling times were 5 min, 10 h and 20 h. The raw materials included 37.5 wt.% of SiO_2, 62.5 wt.% of $CaCO_3$, and the molar ratio was 1.125. The milling speed and ball–to–powder weight ratio were 350 rpm and 10:1, respectively. After this process, the milled powders were calcinated at 1200 °C for 2 h [19].

It is worth noting that steel cups with WC coating and zirconia balls were utilized to conduct the mechanochemical process in the study. In addition, the synthesized compounds were converted to bulk compounds by pressing compounds via a press device (pressure of 300 MPa) and a cylindrical mold (diameter of 5mm and height of 7.5mm). Fig. 1 depicts the mechanism of synthesis of the wollastonite and diopside nano-bioceramics.

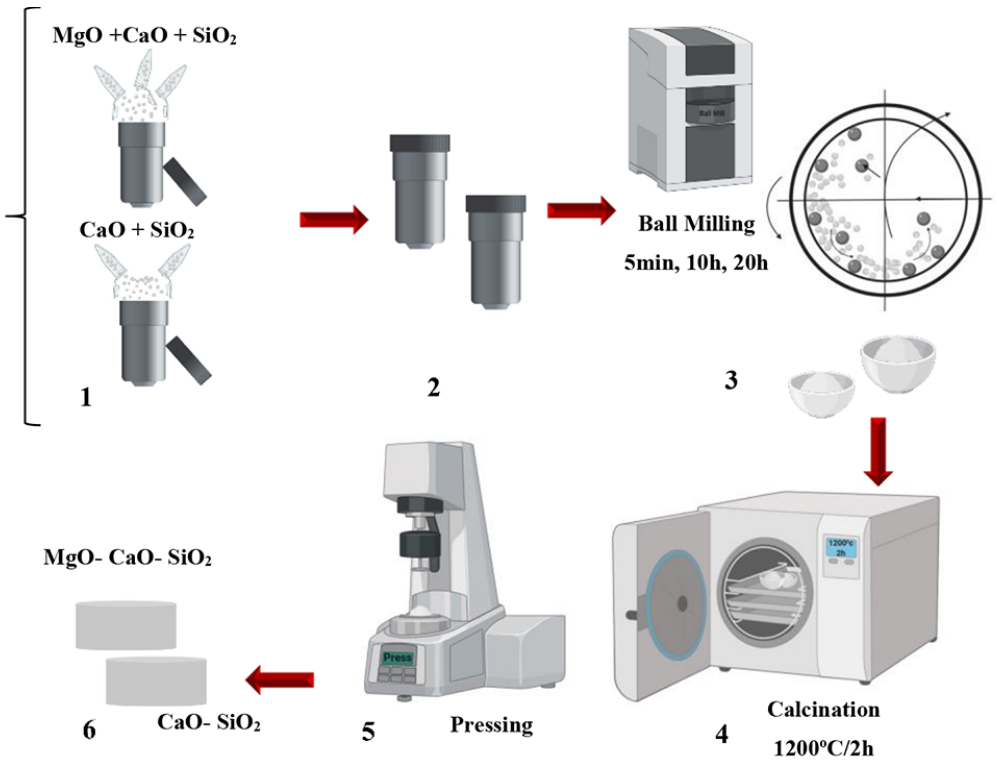

Fig. 1. The mechanism of synthesis of the diopside and wollastonite nano-bioceramics

Table 1. Calculated values of crystallite size by the Scherrer method: (a) diopside and (b) wollastonite

(a)

2θ	Cos(θ)	FWHM	β	D
27.58	0.971	0.1476	0.0025	55
29.86	0.966	0.1968	0.0034	41
30.31	0.965	0.1476	0.0025	56
41.89	0.933	0.1968	0.0034	43
44.37	0.925	0.2460	0.0042	35

(b)

2θ	Cos(θ)	FWHM	β	D
25.987	0.97	0.1476	0.0025	61
27.55	0.971	0.1968	0.0034	47
31.83	0.961	0.1968	0.0034	47
45.88	0.92	0.1968	0.0034	49

2.3. Characterization of diopside and wollastonite

To evaluate the phase structure of the milled and calcinated powders, XRD patterns of these samples were prepared using a PW3040 Philips X-ray diffractometer. The XRD patterns of the samples were obtained via Cu-Kα radiation with a wavelength $\lambda = 1.54018\ A°$ in the ranges of 15–70, 10–60 and 10–50 degrees. To determine the crystallites size of the developed compounds, the width of the present peaks was used in the XRD patterns and Scherrer method. The Scherrer equation [20] is presented as follow:

$$\beta Cos\theta = \frac{K\lambda}{D} \quad (1)$$

where D is the crystallite size, λ is the wavelength, K is the shape factor (about 1), β is the full width at half maximum (FWHM), and θ is half the diffraction angle. To investigate the morphology and micro-structure of the synthesized diopside and wollastonite, scanning electron microscopy (SEM; FEI, Quanta, USA) images were prepared. To examine the chemical composition and distribution of elements of the synthesized diopside and wollastonite compounds, EDS analysis was prepared. To examine the micro-structure and nano-structure of the synthesized diopside and wollastonite, transmission electron microscopy (TEM; EM 208, Philips, the Netherlands) images of the samples were prepared.

2.4. Biomineralization and cell responses

The evaluation of biomineralization and formation of an apatite-like layer on the diopside and wollastonite nano-bioceramics surface was conducted via SBF

solution provided according to the Kokubo method [21]. The nano-bioceramic samples were immersed in 25 ml of the SBF solution (pH=7.4) and were put into an incubator at 37 ℃ for 28 days. After the immersion of the samples for this period, they were washed with distilled water and dried in an oven at 50 °C for 48 h.

The cytotoxicity evaluation was conducted according to ISO 10993-5 standard. The sterilization of the wollastonite and diopside particles was performed in an autoclave. Subsequently, the particles were immersed in Dulbecco's modified eagle medium (DMEM) culture medium using ultrasonic irradiation for 30 min. The MG-63 osteoblast cells (6000 cells) were put into a 24-well plate (TCPS or tissue culture polystyrene) in contact with the culture medium containing the wollastonite and diopside particles. To investigate the cell viability, MTT assay was conducted at 1, 3 and 7 days. Then, the medium was washed with PBS solution, and about 400 µl of the medium and 40 µl of the MTT solutions (5 mg/ml) were added to the culture well, which was kept in an incubator at 37 ˚C for 240 min. The medium was evacuated so that the formazan could be dissolved, and 200 µl of dimethyl sulfoxide (DMSO) was added to the wells. Optical absorption was evaluated over 570 nm.

To examine the deposited calcium rate by the MG-63 osteoblast cells, alizarin red staining was used for 7 and 14 days. After culturing the MG-63 osteoblast cells for 7 and 14 days, the cells were fixed with formaldehyde (4%), and then the prepared alizarin red staining (1%) was added to Tris buffer solution with pH=8 for 15 min. The well plate containing cells was washed with PBS solution several times.

To investigate the alkaline phosphatase enzyme activity rate at 3, 7 and 14 days of cell culture on the diopside and wollastonite compounds, at first, the Ripa solution was used in the entire protein extraction. After extracting the perfect cell culture, 20 µl of the Ripa solution was poured on the bioceramics, and they were pipetted for 10 min. The Ripa solution was centrifuged at 14000 rpm for 10 min and was kept at 4 °C. Afterwards, for each 20 µl of Ripa solution, 1 mM of reagent No.1 of kit of alkaline phosphatase was added to the samples, and they were put into the incubator at 37 °C for 1 min. Then, 250 µl of reagent No.2 was added to the samples, and the same process was repeated. After 1, 2, and 3 min, optical absorption was read over 405 nm, and then its difference was determined from the last minute. Finally, these three differences and their mean were calculated, and the final number was multiplied by the factor 3433.

2.5. Statistical analysis

The experiments were performed for n=3. All data were suggested as mean ± SD. One-way analysis of variance (ANOVA) was used to compare the results. A p-value of less than 0.05 was determined to be statistically significant.

3. Results and discussion

Figs. 2a-c present the XRD patterns of the milled powders of materials like MgO, $CaCO_3$ and SiO_2 at 5 min, 10 h, and 20 h. In Fig. 2a, the milled powers at 5 min, only magnesium oxide (MgO) (JCPDS 01–087–0652) and calcium carbonate ($CaCO_3$) phase (JCPDS 01–081–2027) were observed, and by extending the milling time for 10 h (Fig. 2b), the peaks widened. The phenomenon is due to the decrease in the crystallite size and the increase in the lattice strain during the mechano-chemical process. By extending the milling time for 20 h, because the raw materials became amorphous, the peaks related to the calcium carbonate phase gradually decreased (Fig. 2c, milling time=20 h). In the mechano-chemical (ball milling) process, much energy is applied to the powder particles, and internal energy (ΔU) is highly increased. A lot of strains in the system present serious motion of dislocations, causing different structural defects like dislocations, vacancies, stacking fault, and increasing the development of grains boundary. Finally, these changes increase the speed of the reactions between the milled particles. The transformation of the milled powder structure is so high that the primary lattice is perfectly altered. During the milling process, various phenomena like mixing and chemical reactions in contact with particle levels might occur, causing chemical reactions to take place during the milling process and the reactivity of the milled product to increase [22].

The main peaks of SiO_2 phase are not identifiable in the ranges of diffracted angles of 20–30 degrees in the XRD patterns (Figs. 2a-c). As a result of the milling process for 20 h (Fig. 2c), the pattern lacked the diopside phase ($CaMgSi_2O_6$). Subsequently, to develop the diopside phase, the milled powders were calcinated at 1200 ℃ for 2 h.

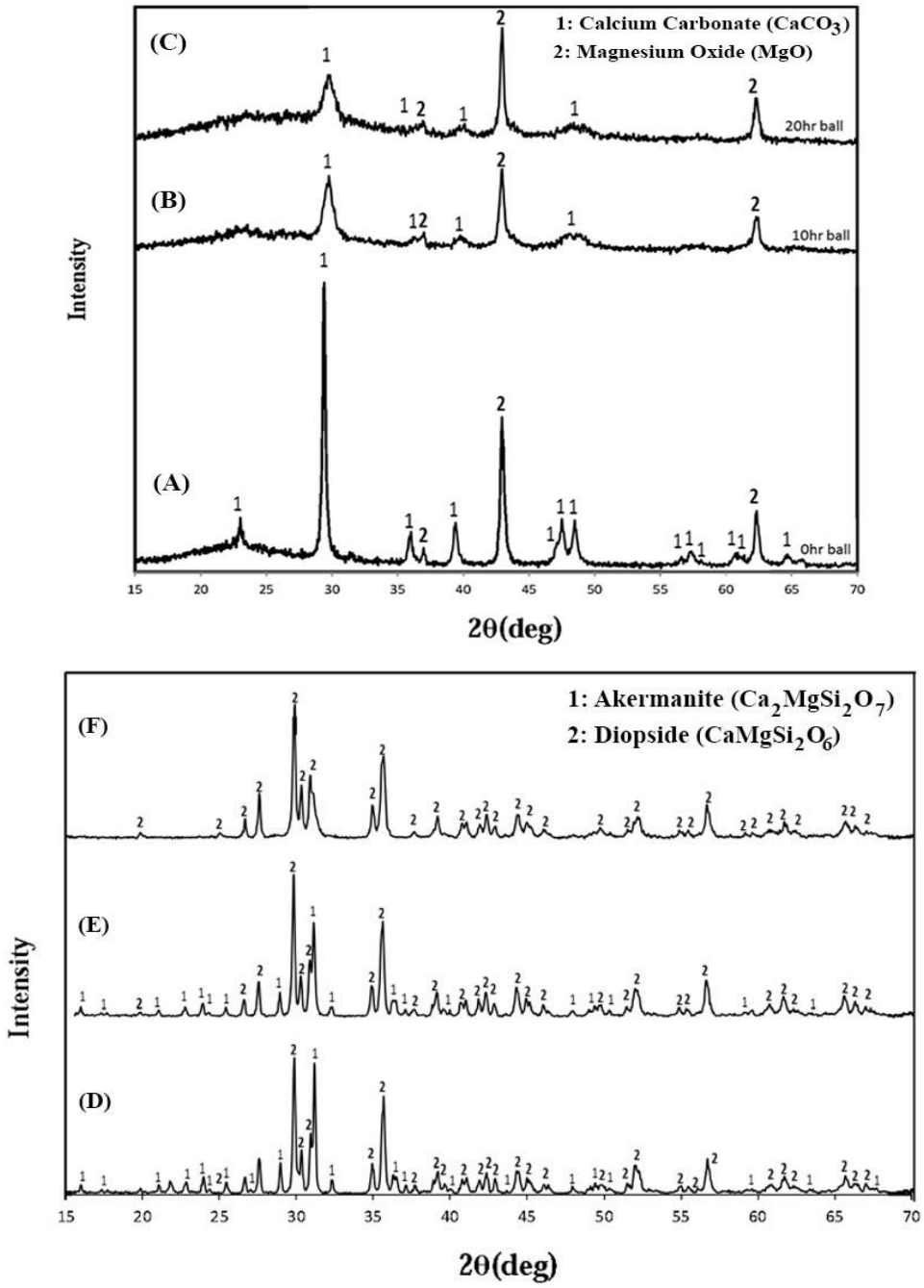

Fig. 2. XRD patterns of the milled powders among raw materials related to the diopside phase: (a) 5 min, (b) 10 h, and (c) 20 h, XRD patterns of the sintering process of the milled powders at 1200 ℃ for formation of diopside phase: (d) 5 min, (e) 10 h, and (f) 20 h

Figs. 2d-f presents the XRD patterns of the calcination process of the milled powders at 5 min, 10 h, and 20 h at 1200 ℃. In the calcinated sample of the milled powder at 5 min (Fig. 2d), the diopside ($CaMgSi_2O_6$) phase (JCPDS 01–071–1494) with mono-clinic structure was developed, and akermanite ($Ca_2MgSi_2O_7$) phase (JCPDS 01–077–1149) with a tetragonal structure was observed in the XRD pattern of this sample (Fig. 2d).

In the calcinated sample of the milled powder at 10 h (Fig. 2e), the peaks related to the diopside phase increased, and those related to the akermanite phase decreased (Fig. 2e). In the calcinated sample of the milled powder at 20 h (Fig 2f), the pattern lacked the akermanite phase, and only the diopside phase was clearly observed because of appropriate milling time (20 h) among the raw materials. Formation of the diopside phase is according to relations 2 and 3:

$$CaCO_3 \rightarrow CaO + CO_2 \quad (2)$$

$$CaO + 2SiO_2 + MgO \rightarrow CaMgSi_2O_6 \quad (3)$$

To obtain the optimum milling time, the milling process was conducted among raw materials like $CaCO_3$ and SiO_2 for 5 min, 10 h and 20 h. Figs. 3a-c indicated the XRD patterns related to the milled powders at 5 min, 10 h and 20 h. In the XRD pattern in Fig. 3a, only the phases related to the raw materials like $CaCO_3$ exist, and by increasing the milling time to 10 h, the peaks widen (Fig. 3b) because of a

decrease in the crystallite size and an increase in the lattice strain during the milling process [23]. In this pattern (Fig. 3b), only the phase related to the raw materials compound was observed. By increasing the milling time to 20 h (Fig. 3c), because the raw materials became amorphous, some peaks related to $CaCO_3$ phase were gradually removed and were increased 20–30 degrees. The main peaks of the SiO_2 phase were in the diffracted angles of 20–30 degrees, which was not identifiable in the XRD patterns (Figs. 3a-c). The patterns lacked the wollastonite phase. Figs. 3d-f exhibited the XRD patterns of the calcination process of the milled powders (5 min, 10 h and 20 h of the milling time) at 1200 ℃ for 2 h.

In Figs. 3d,e, the wollastonite ($CaSiO_3$) phase (JCPDS 01-073-1110) and rankinite phase ($Ca_3Si_2O_7$) (00-011-0317) were observed because of extending the milling time to 20 h among the raw materials. The formation of the wollastonite phase is according to relations 2 and 4.

$$CaO + SiO_2 \rightarrow CaSiO_3 \quad (4)$$

To calculate the crystallite size of the synthesized diopside and wollastonite, the Scherrer method was used. Table 1 presents the calculated values for the synthesized diopside and wollastonite obtained by calcination and mechano-chemical processes (milling time: 20 h). According to the results, the mean crystallite sizes of diopside and wollastonite nano-bioceramics were 46 and 51 nm, respectively.

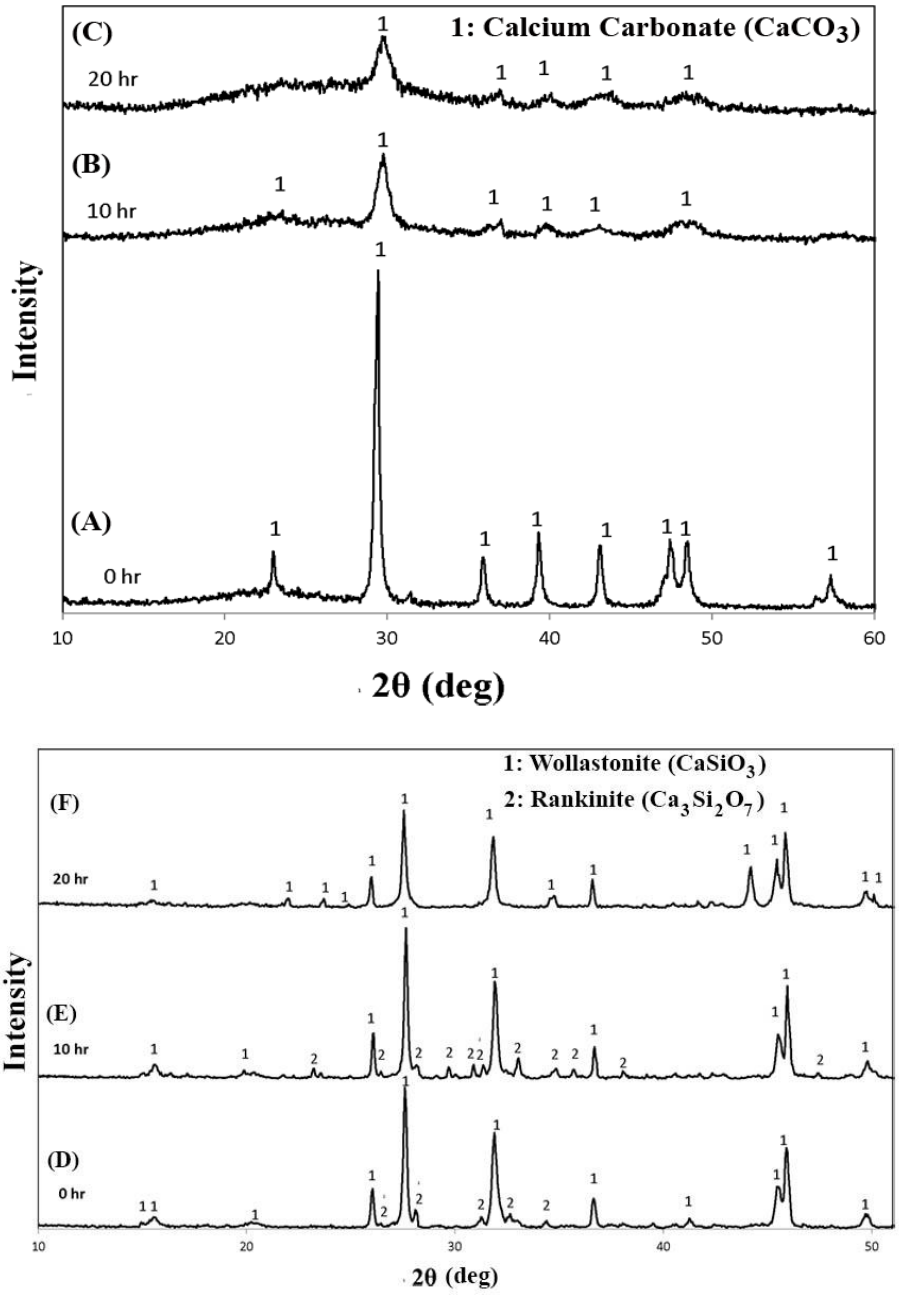

Fig. 3. XRD patterns of the milled powders among raw materials related to the wollastonite phase: (a) 5 min, (b) 10 h, and (c) 20 h, XRD patterns of the sintering process of the milled powders at 1200 ℃ for wollastonite phase formation: (d) 5 min, (e) 10 h, and (f) 20 h

Fig. 4a presents the morphology related to the synthesized diopside. In the SEM image, the diopside structure is continuously in a trapezoidal shape. According to Fig. 4b and Table 2, the results of EDX analysis of the synthesized diopside showed that oxygen (O), silicon (Si), calcium (Ca) and magnesium (Mg) elements are the constituent elements of diopside. They also proved the non–availability of the synthesized compound. Additionally, there are Mg^{2+}, Si^{4+}, and Ca^{2+} ions, meaning that as a result of the milling process, proper primary distribution of the raw materials occurred, causing uniform diopside to develop.

Fig. 4c presents the morphology relevant to the synthesized wollastonite. The SEM image showed the morphology of the wollastonite structure continuously in a plate shape. According to Fig. 4d and Table 3, the EDX results of the synthesized wollastonite showed that oxygen (O), silicon (Si), and calcium (Ca) were the constituent elements of the wollastonite, and its non– availability was proved by the EDX analysis. It reveals that Si^{4+} and Ca^{2+} ions exist, showing an appropriate primary distribution among the raw materials after the milling process, which made uniform wollastonite.

(a)

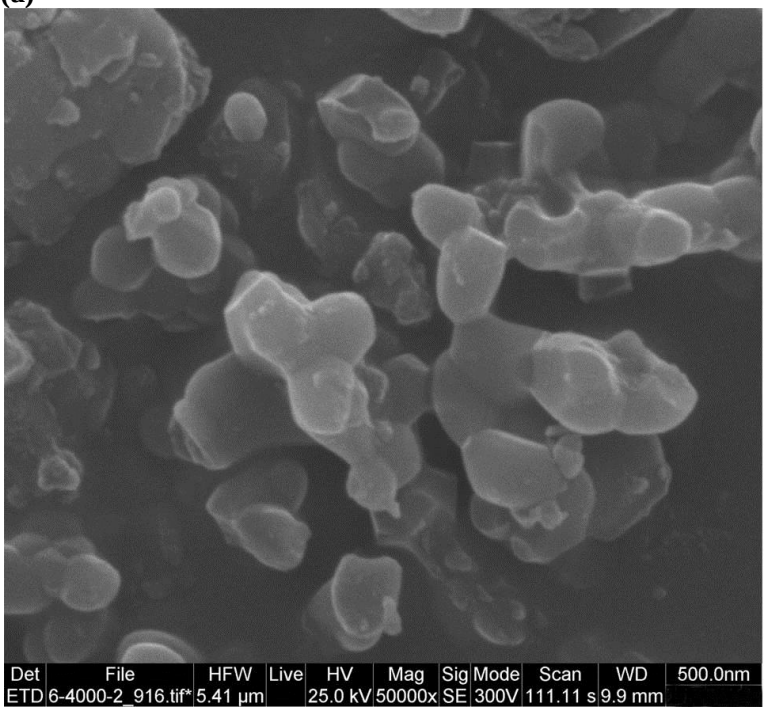

(b)

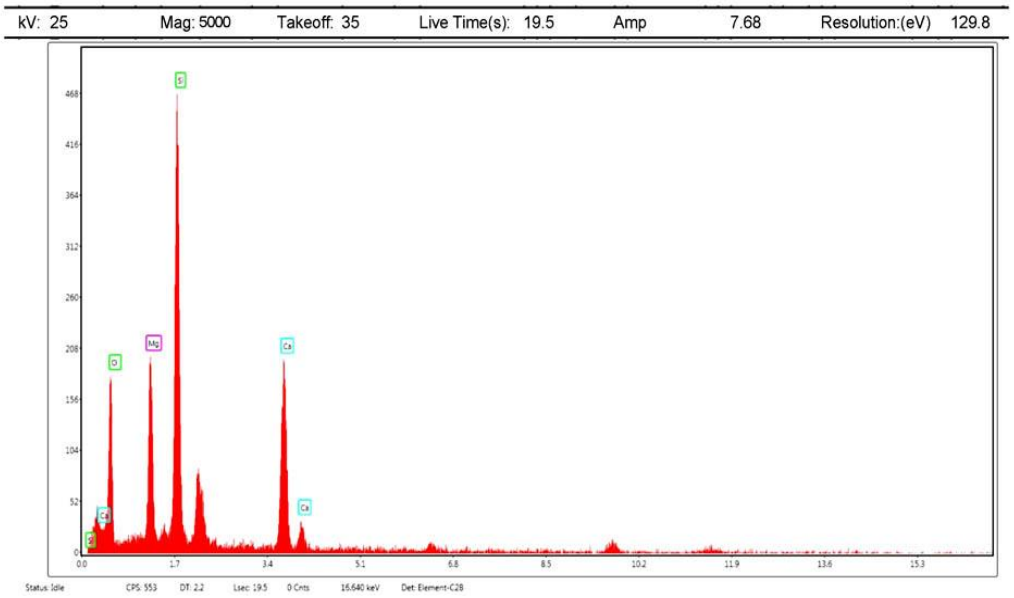

(c)

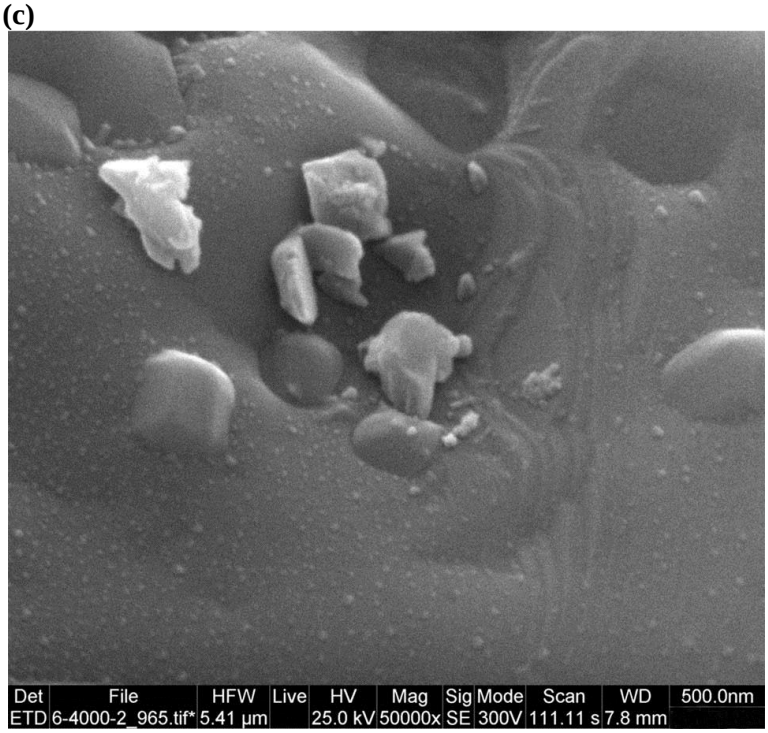

(d)

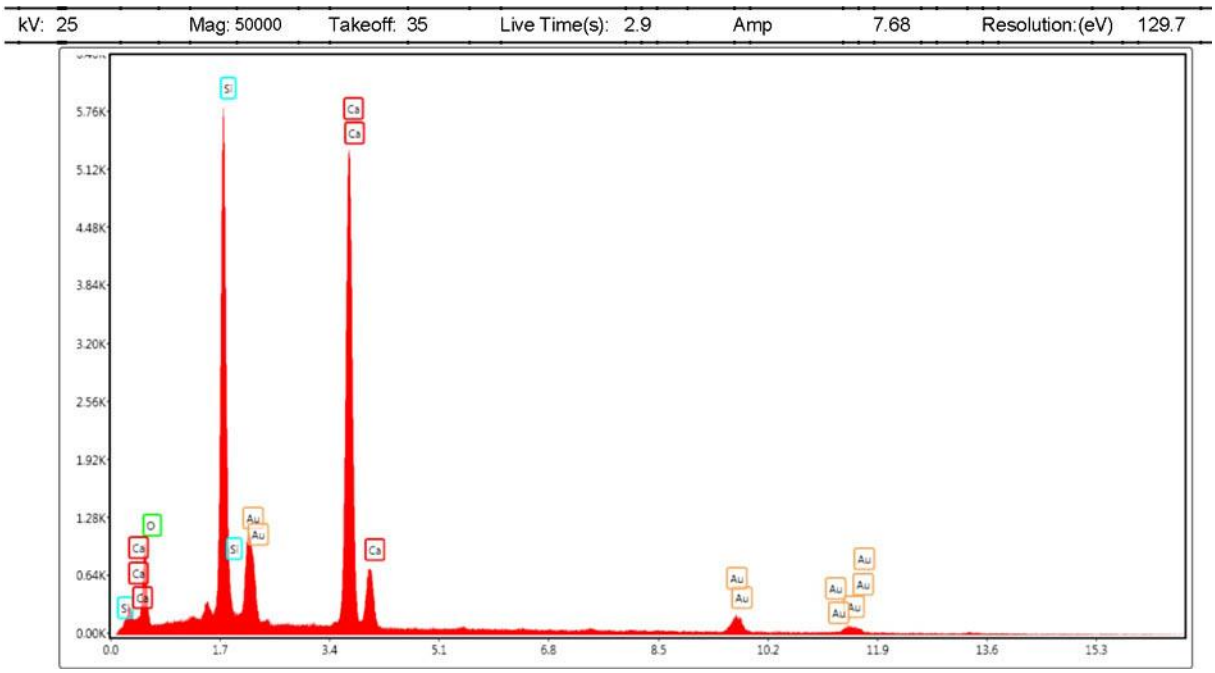

Fig. 4. (a) SEM image of diopside, (b) EDX analyis of diopside, (c) SEM image of wollastonite and (d) EDX analysis of wolastonite

Table 2. Results of EDX analysis of synthesized diopside

Element	Weight%	Atomic %	Net Int.
O	41.79	56.95	68.47
Mg	14.46	12.97	86.53
Si	27.02	20.98	211.76
Ca	16.73	9.1	109.25

Figs. 5a-c exhibited the TEM images of the synthesized diopside in which the particle sizes of the diopsides were smaller than 100 nm. TEM images showed the formation of interconnected agglomerates, and the range of nanostructure was observed. In other words, TEM images suggested

that the real size of the diopside was less than 80 nm. However, it can be stated that the average size was about 80 nm due to developing larger particles as a result of particle agglomeration. It can be concluded that the synthesis of diopside nano-bioceramic by combining mechano-chemical and calcination processes is successful.

(a)

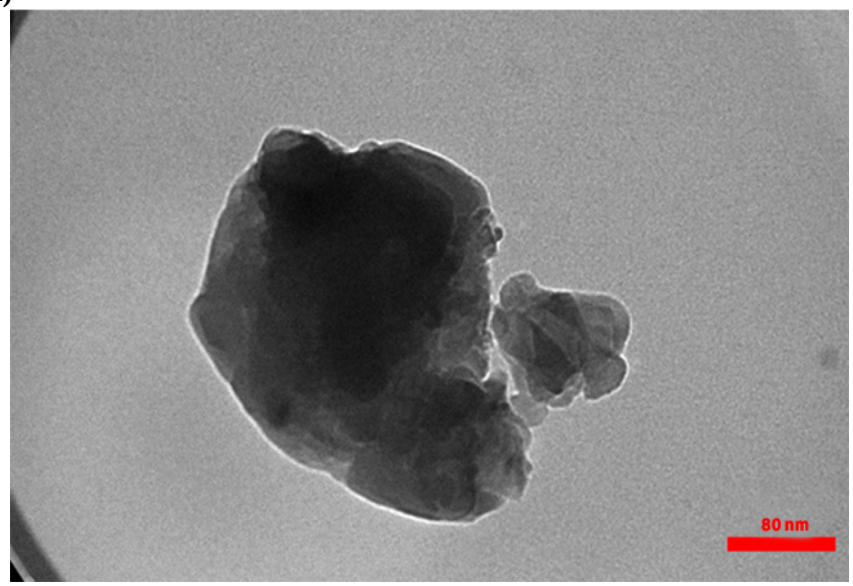

(b)

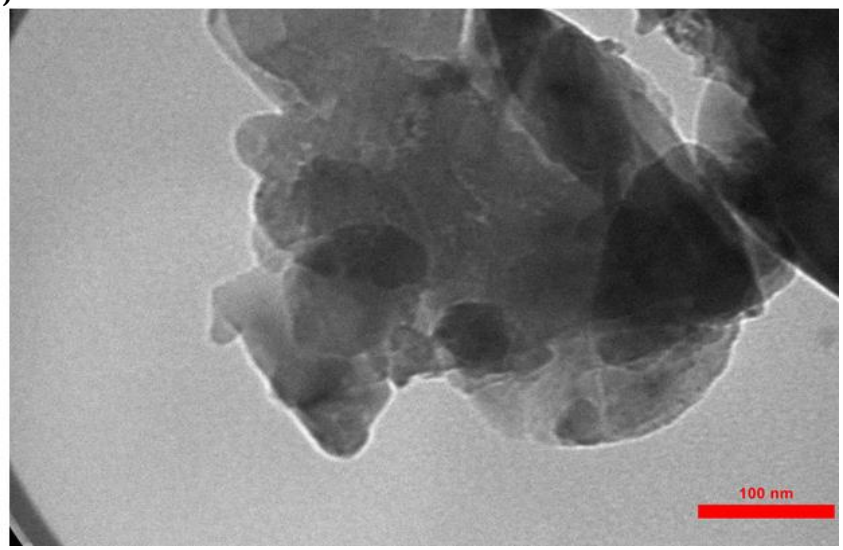

(c)

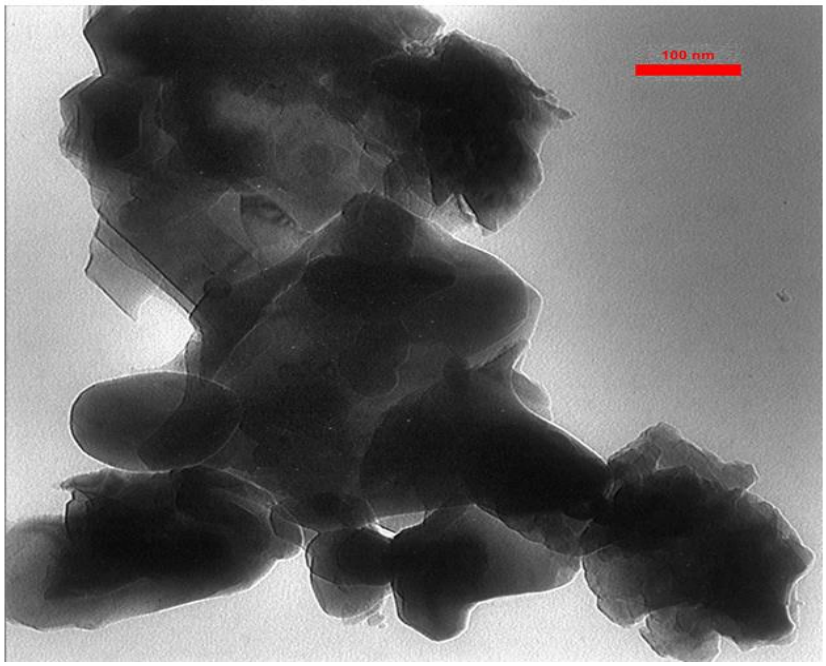

Fig. 5. TEM images of diopside

Table 3. Results of EDX analysis of synthesized wollastonite

Element	Weight%	Atomic %	Net Int.
O	26.44	48.56	2583.16
Si	21.06	22.03	18004.71
Ca	36.95	27.09	22010.61
Au	15.54	2.32	1217.38

Figs. 6a,b illustrate the TEM images of the synthesized wollastonite in which the sizes of the wollastonite were smaller than 100 nm. TEM images showed the development of connected agglomerates, and the range of nanostructure was observed. Moreover, TEM images of the wollastonite indicated that the actual size of wollastonite was almost less than 80 nm. In other words, it can be expressed that the mean size was about 80 nm because of the formation of larger particles resulting from particle agglomeration. It can be concluded that the synthesis of wollastonite nano-bioceramic using a combination of mechano-chemical and calcination processes is successful.

(a)

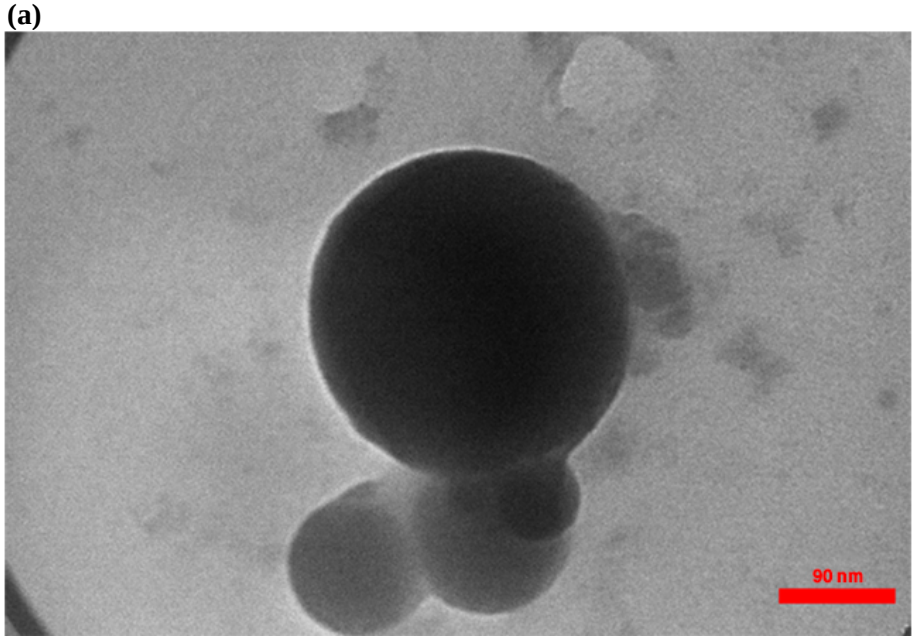

(b)

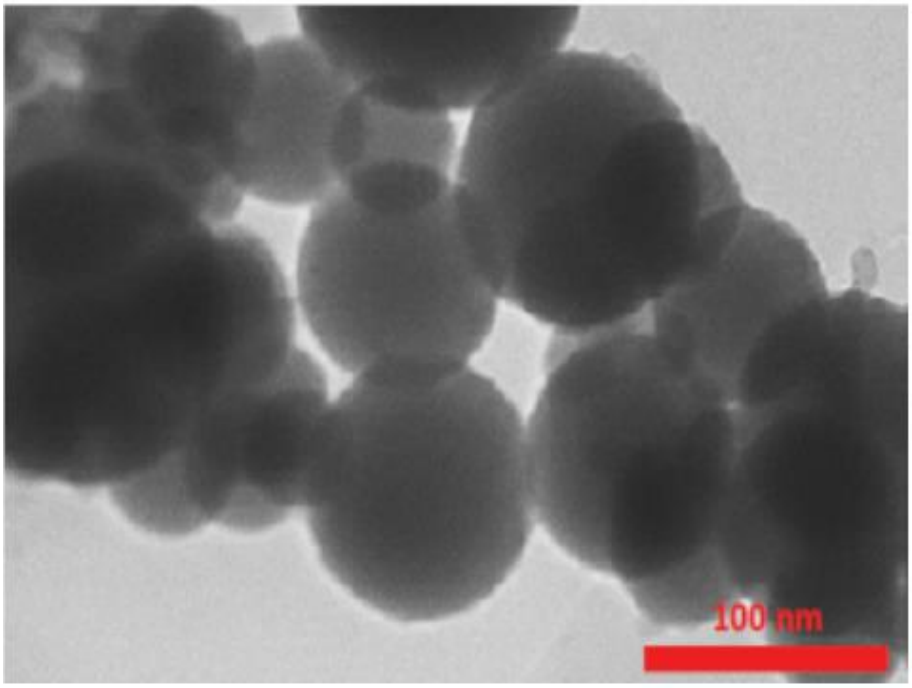

Fig. 6. TEM images of wollastonite

Table 4. Results of the EDX analysis of the synthesized wollastonite bio-mineralization

Element	Weight %	Atomic %	Net Int.
O	46.31	65.68	45.68
P	23.58	17.05	168.82
Ca	30.11	18.28	177.6

Fig. 7a presents the SEM image of wollastonite nano-bioceramic immersed in SBF for up to 28 days and suggests the development of an extensive apatite-like layer on the surface of wollastonite. The EDX analysis (Fig. 7b and Table 4) confirms the presence of Ca, P, and O. Finally, it proves the development of a $CaO\text{-}P_2O_5$ film on the surface of the nano-bioceramic. Actually, the EDX analysis expresses high values related to P and Ca, resulting in the creation of an apatite-like layer on the surface of wollastonite. Fig. 7c shows the SEM image of diopside nano-bioceramic immersed in SBF for up to 28 days, and Fig. 7c depicts the development of an apatite-like layer on the surface of the diopside. The issue was confirmed via EDX analysis (Fig. 7d and Table 5), which presented a high atomic percentage of Ca and P, proving the development of a $CaO\text{-}P_2O_5$ film on the surface of the diopside nano-bioceramic. It can be discussed that Ca^{2+} and Mg^{2+} cause hydrolysis reaction of the silica group to be conducted, generating the initial apatite crystals, and causing the Ca^{2+} and Mg^{2+} ions to be released. The ions migrated to the silica surface, and finally, a $CaO\text{-}P_2O_5$ film was developed on the silica surface, and apatite crystals were nucleated [24, 25]. Concerning the discussions, it is concluded that wollastonite and diopside are bioactive nano-bioceramics that can possess bone tissue bio-mineralization for bone tissue engineering applications.

(a)

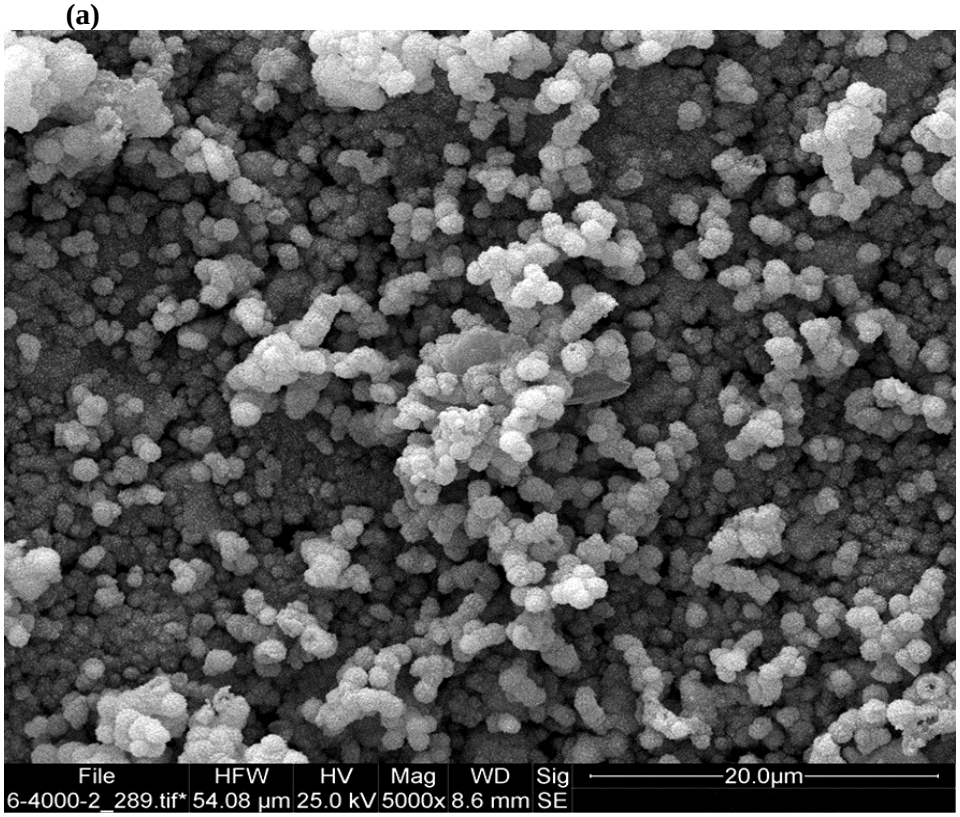
File
6-4000-2_289.tif*
HFW
54.08 µm
HV
25.0 kV
Mag
5000x
WD
8.6 mm
Sig
SE
20.0µm

(b)

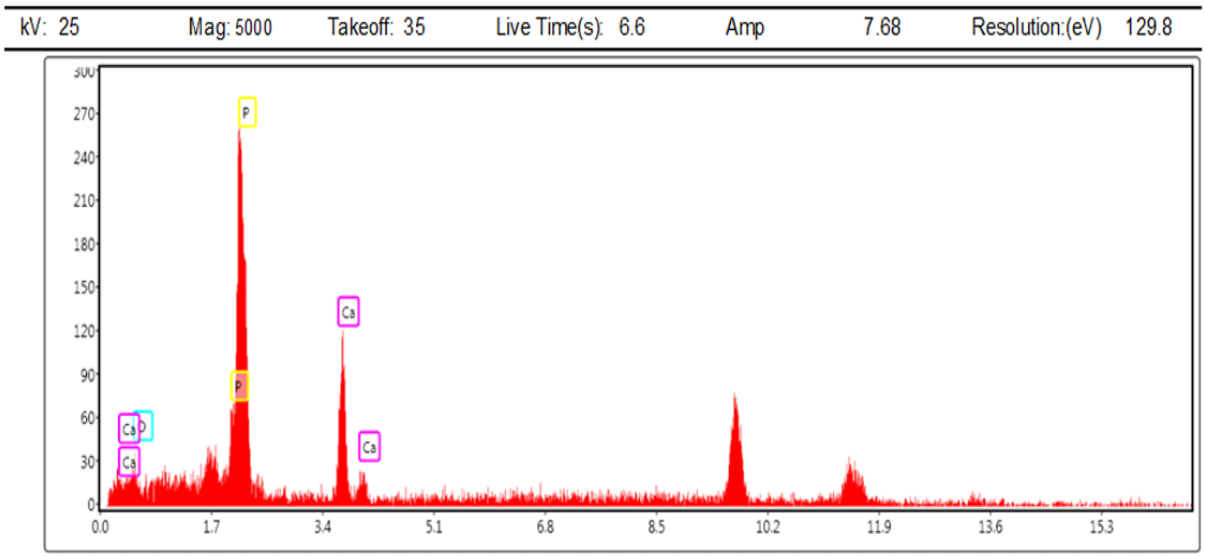
kV: 25
Mag: 5000
Takeoff: 35
Live Time(s): 6.6
Amp
7.68
Resolution:(eV)
129.8
P
Ca
P
Ca
O
Ca
Ca
0.0
1.7
3.4
5.1
6.8
8.5
10.2
11.9
13.6
15.3

(c)

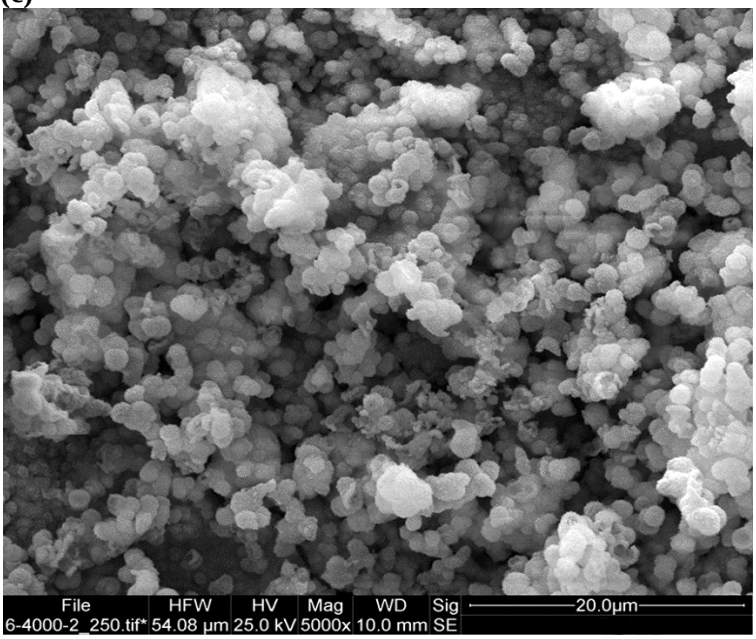

(d)

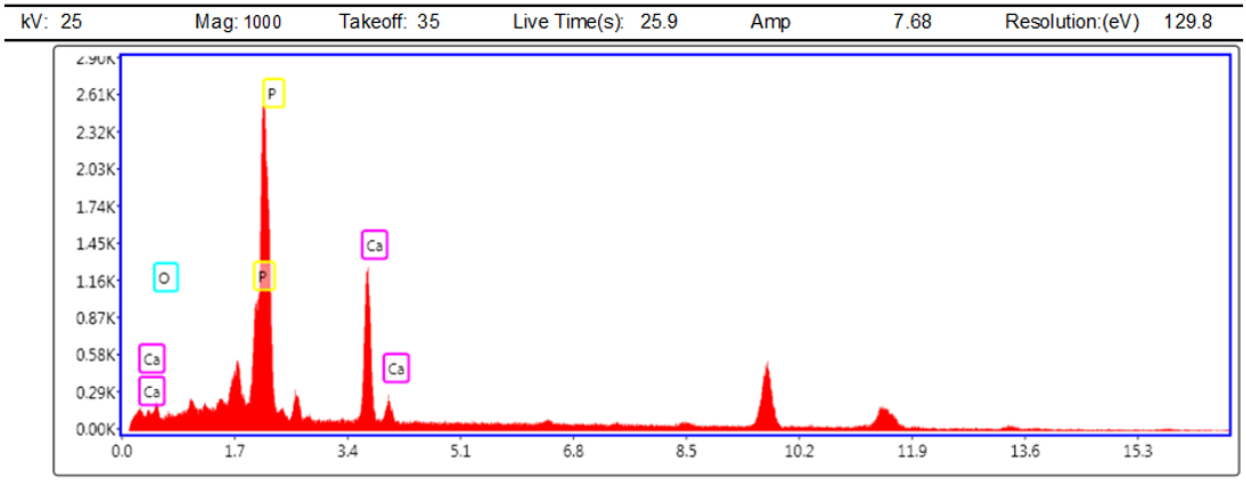

Fig. 7. (a) SEM image of wollastonite in immersed SBF for up to 28 days, (b) EDX analysis, (c) SEM image of diopside immersed in SBF for up to 28 days, (d) EDX analysis

Table 5. Results of the EDX analysis of the synthesized diopside bio-mineralization

Element	Weight %	Atomic %	Net Int.
O	36.59	56.08	80.53
P	28.41	21.42	497.56
Ca	35.1	23.76	559.6

Fig. 8 depicts the mechanism of apatite formation. Generally, morphology related to apatite crystals is in the form of needle-like and cauliflower-like shapes on the surface of the nano-bioceramics. On the other hand, EDX analyses showed that Ca, P, and O elements indicate the formation of Ca–P–O on the surface of the nano- bioceramics. With regard to SEM images and EDX analyses, it can be concluded that the development of an apatite-like layer and apatite crystals on the surface of the nano-wollastonite and nano-diopside was carried out correctly. This issue clearly presents the bioactivity of the synthesized compounds.

Fig. 9 shows the results of cell viability of wollastonite and diopside nano-bioceramics. The cell viability assay related to nano-bioceramics was conducted by utilizing MG-63 osteoblast cells and 1, 3, and 7 days of cell culture. It suggests a meaningful difference ($p<0.05$) in the cell viability of nano-bioceramics. Cell viability and proliferation of MG-63 osteoblast cells enhanced after 7 days. It verified the compatibility cells of wollastonite and diopside

due to stimulating the MG-63 osteoblast cells via wollastonite and diopside, an effective factor for the enhancement of cell growth, viability, and proliferation. Moreover, nano-bioceramics lacked cytotoxicity by the MG-63 osteoblast cells.

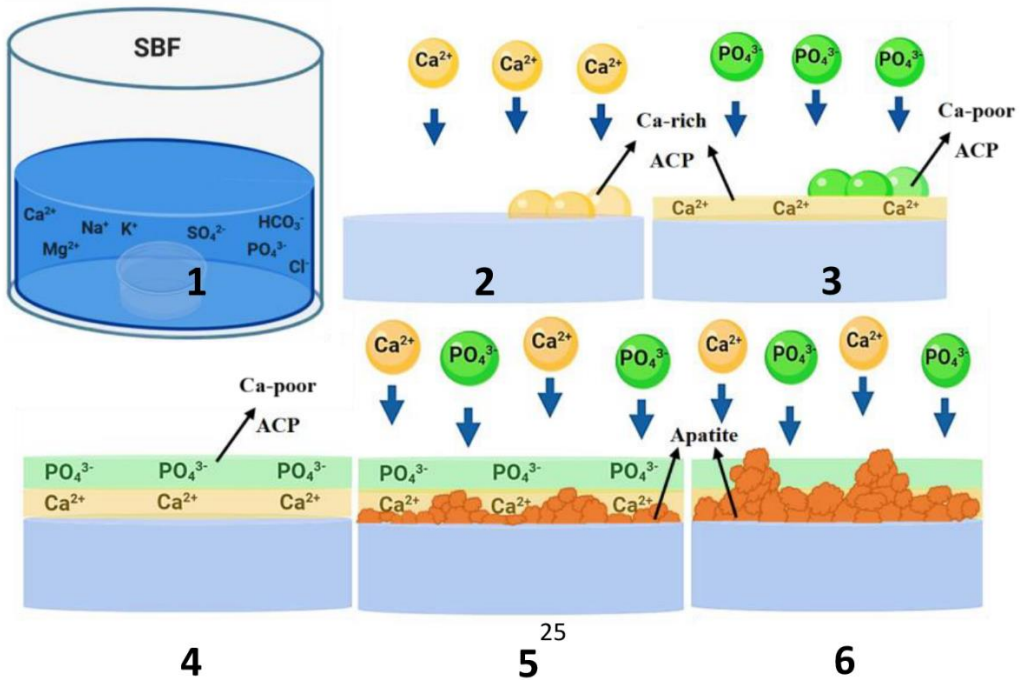

Fig. 8. The mechanism of apatite formation on bioactive diopside and wollastonite nano-bioceramics

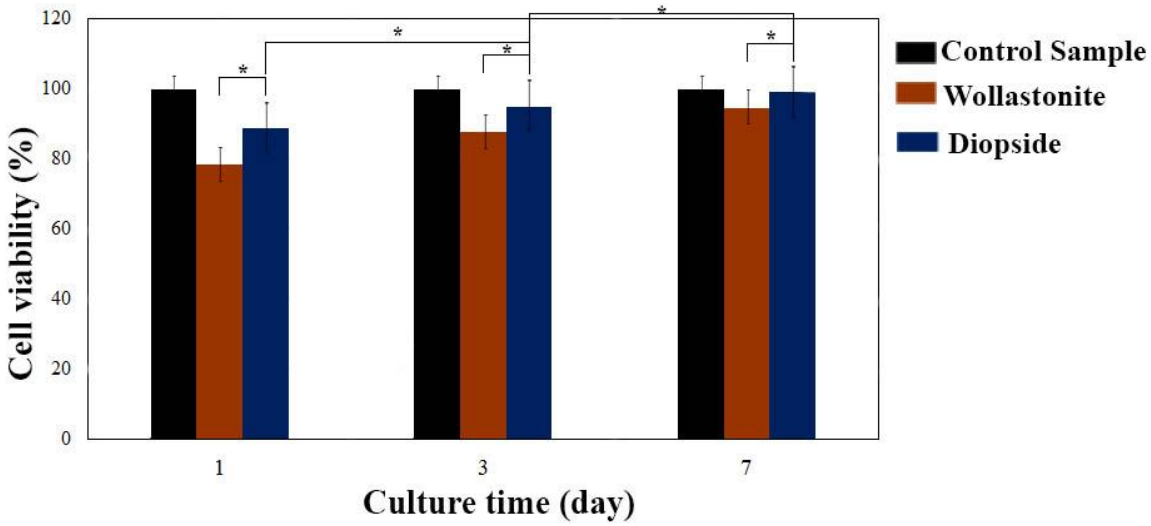

Fig. 9. Results of cell viability related to wollastonite and diopside nano-bioceramics

Figs. 10a,b present the optical microscope images of the culture medium, including MG-63 osteoblast cells and diopside nano-bioceramic after alizarin red staining for 7 and 14 days. After 7 days, red veins (Fig. 10a) are observed. Fig. 10b presents an optical microscope image after 14 days of alizarin red staining. The majority of areas in the image are red, showing that calcium activity in the diopside increased after 14 days. In fact, diopside increased the secretion of calcium in the cells causing the Ca^{2+} ions to be released from the cell membrane. It persuaded the MG-63 osteoblast cells to secrete calcium, indicating the high bioactivity of diopside. Similarly, Figs. 10c,d present the optical microscope images of the culture medium, including MG-63 osteoblast cells and wollastonite nano-bioceramic after 7 and 14 days of alizarin red staining. After 14 days of alizarin red staining, calcium activity increased in wollastonite. In fact, wollastonite caused calcium secretion in the cells to increase, suggesting the release of the Ca^{2+} ion from the cell membrane. Accordingly, wollastonite persuaded the MG-63

osteoblast cells to secrete calcium, showing that wollastonite is bioactive nano-bioceramic.

Fig. 10e presents the optical absorption (nm) according to the culture time (day) diagram after alizarin red staining related to diopside and wollastonite. According to the results, there was a meaningful difference ($p < 0.05$) for wollastonite and diopside at 7 and 14 days.

Fig. 10e proves that increasing calcium activity related to two compounds after 14 days of alizarin red staining is much better and more outstanding than increasing calcium activity after 7 days of alizarin red staining related to two compounds. It can be expressed that alizarin red staining showed that MG-63 osteoblast cells in contact with diopside nano-bioceramic and culture medium were stimulated so that Ca^{2+} was released from the cell membrane, and therefore, more red veins and high absorption related to calcium activity. Moreover, with regard to the results of alizarin red staining between diopside and wollastonite, it is concluded that diopside has offered more acceptable and excellent performance compared to wollastonite. In fact, the bioactivity of diopside was higher than that of wollastonite. Generally, when Mg^{2+} was added to the calcium silicate network, chemical bonds such as ionic and covalent bonds become stronger in $CaO–SiO_2–MgO$ system. In other words, adding Mg^{2+} causes the chemical stability of the calcium-silicate network. The issue is effective in improving the mechanical and biological properties of nano-bioceramics. One of the biological parameters is bioactivity. Therefore, the bioactivity of the diopside is much better in comparison to that of the wollastonite.

(a)

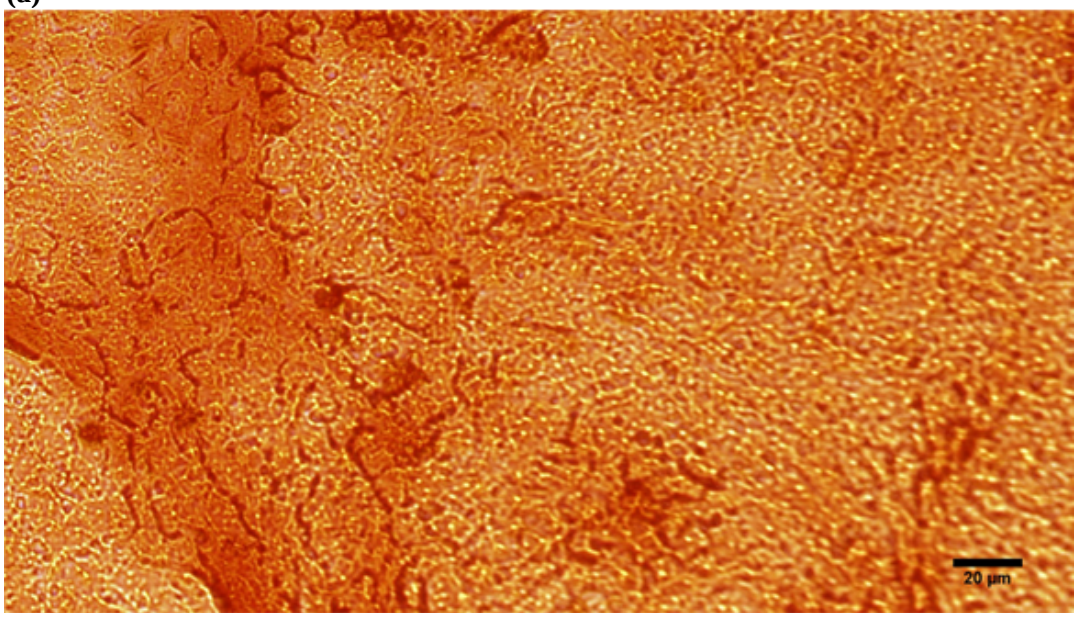

(b)

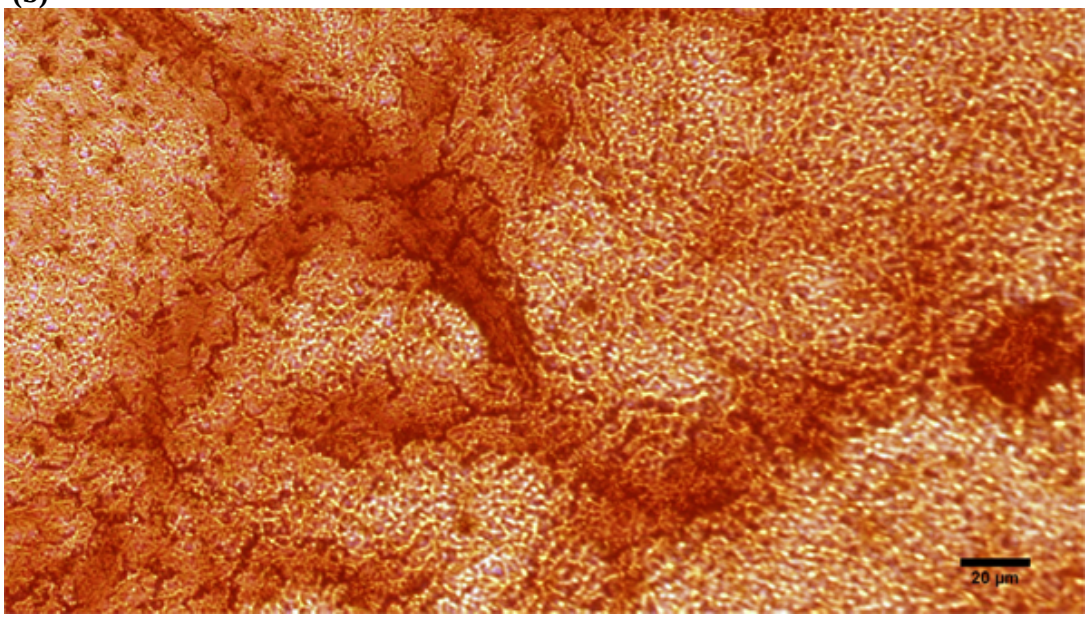

(c)

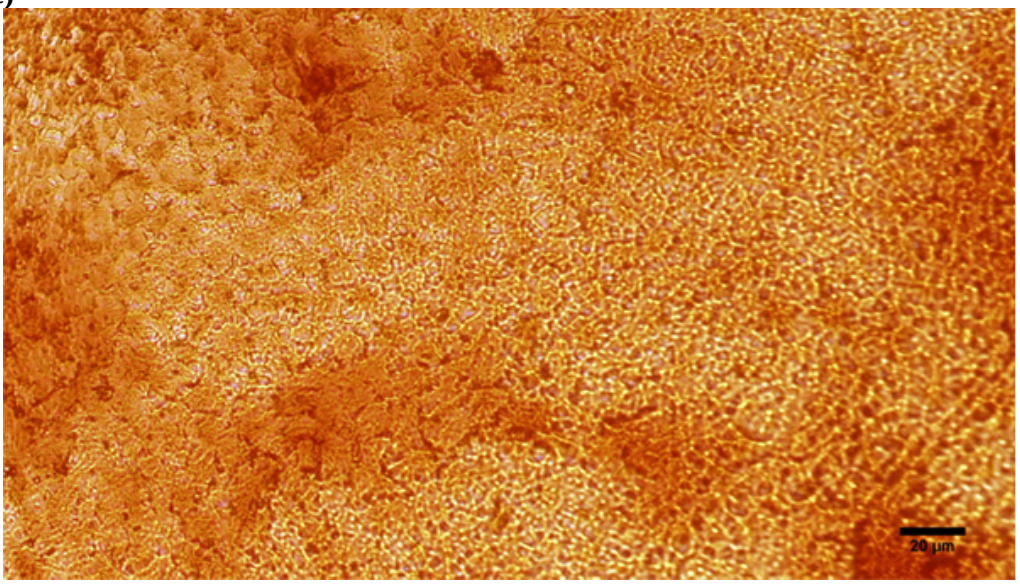

(d)

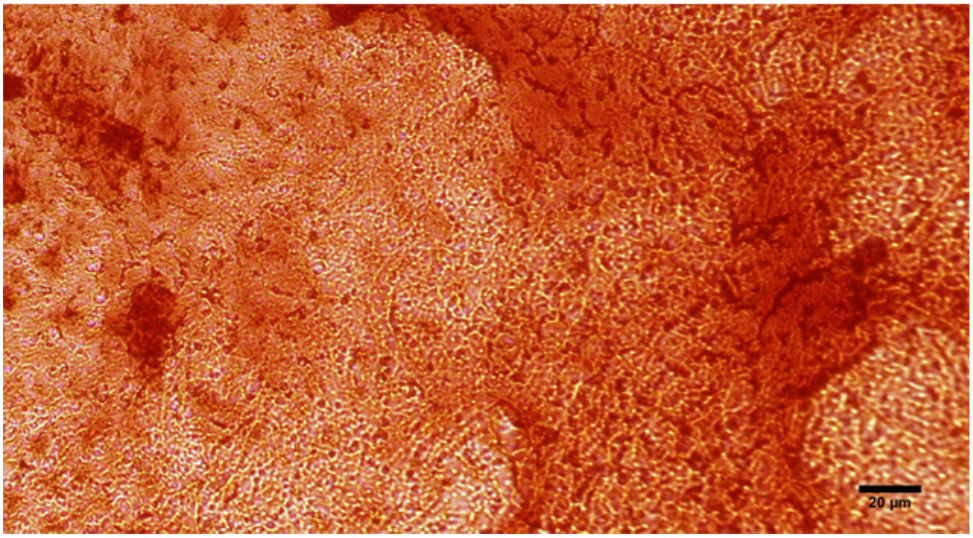

(e)

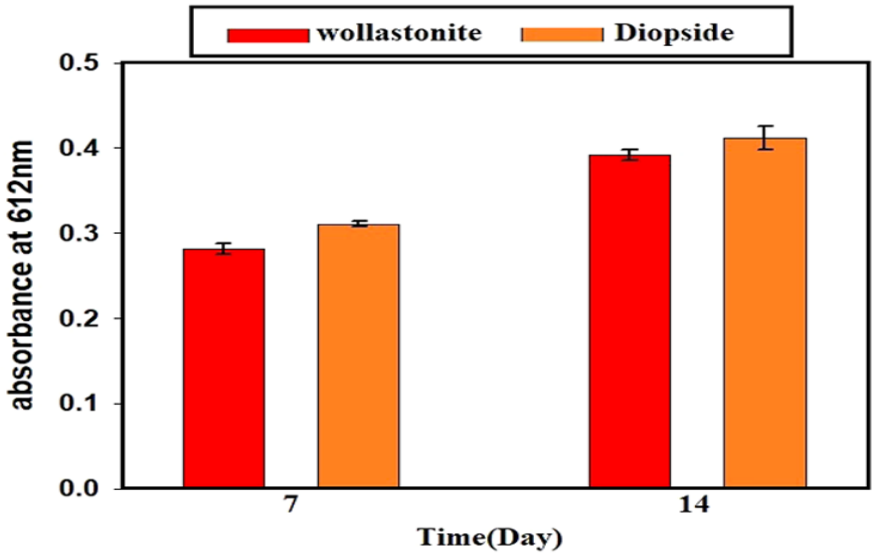

Fig. 10. (a) and (b) Optical microscope images of the culture medium (MG–63 osteoblast cells and diopside) obtained by alizarin red staining, (c) and (d) Optical microscope images of the culture medium (MG–63 osteoblast cells and wollastonite) obtained by alizarin red staining, and (e) diagram of optical absorption according to the culture time after alizarin red staining relevant to diopside and wollastonite compounds

Fig. 11 presents the diagram of the ALP rate according to culture time of diopside and wollastonite after culturing for 3, 7, and 14 days. According to the results, there was a meaningful difference ($p<0.05$) for wollastonite and diopside at 3, 7, and 14 days. As can be observed, high alkaline phosphatase enzyme activity increased in the presence of diopside and wollastonite after 14 days of culture. Moreover, the enzyme possesses better activity in the presence of diopside compared to its activity in the presence of wollastonite. The obtained results showed that the secretion of the alkaline phosphatase enzyme was in contact with diopside and wollastonite compounds from inside the osteoblast cells, causing the formation and restoration of the bone tissue to be accelerated. Diopside had high cell responses compared to wollastonite. This can refer to the incorporation of Mg^{2+} into the calcium-silicate network and, consequently, stability of the network and the enhancement of the cell responses. With respect to cell responses of diopside and wollastonite, it can be concluded that they can serve as potential candidates to apply in bone tissue engineering.

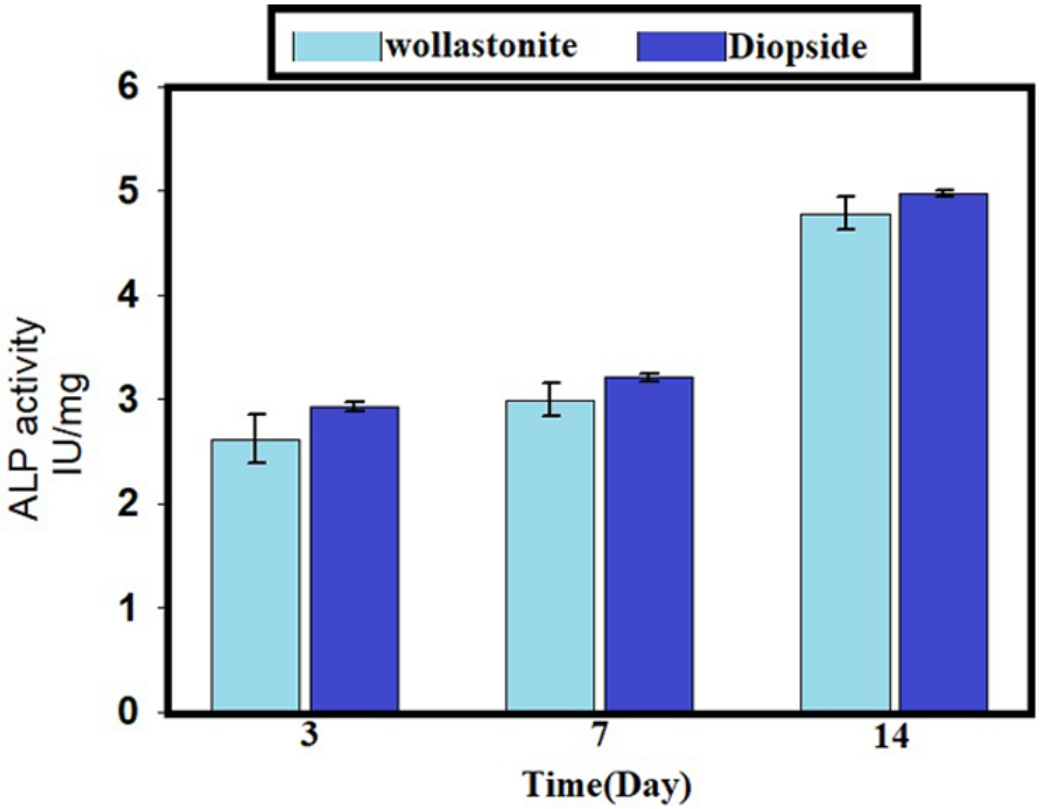

Fig. 11. Diagram of ALP rate–culture time after culturing for 3, 7 and 14 days related to diopside and wollastonite compounds

4. Conclusions

Synthesis and characterization of diopside and wollastonite nano-bioceramics were successfully performed via mechano-chemical and calcination processes. The phase analyses showed that the diopside and wollastonite phases were developed in the $CaO–SiO_2–MgO$ ternary and $CaO–SiO_2$ binary systems after milling for 20 h and calcination at 1200. The TEM images proved that diopside and wollastonite possessed nanostructured with a mean size of about 80 nm due to mechano-chemical and calcination processes. The results related to bio-mineralization and cell responses verified appropriate tissue biomineralization of wollastonite and diopside using the apatite-like layer on the surface of nano-bioceramics. Cell responses of wollastonite and diopside resulted in non-cytotoxicity by the MG-63 osteoblast cells, which confirmed their viability and cell proliferation. Alizarin red staining related to diopside and wollastonite proved high bioactivity and tissue bio-mineralization. The enhancement of the ALP enzyme related to diopside and wollastonite occurred in contact with the MG-63 osteoblast cells. With regard to the existence of Mg^{2+} in the calcium-silicate network and the stability network, diopside exhibited high biological and cell responses compared to wollastonite. Finally, wollastonite and diopside can be suggested as bioactive and biocompatible nano-bioceramics for bone tissue engineering.

References

[1] A. Borger, P. Supancic, R. Danzer, “The ball on three balls test for strength testing of brittle discs:

stress distribution in the disc", Ceram. Eur. Soc. J., Vol. 22, 2002, pp. 1425-1436.
[2] R. Damani, R. Gstrein, R. Danzer, "Critical notch – root radius effect in SENB – S fracture toughness testing", Eur. Ceram. Soc. J., Vol. 16, 1996, pp. 695-702.
[3] P.N. De Aza, Z.B. Luklinska, A. Martinez, M.R. Anseau, F. Guitian. S. De Aza, "Morphological and structural study of pseudowollastonite implants in bone", Microsc. J., Vol. 197, 2000, pp. 60-67.
[4] S.V. Dorozhkin, "Bioceramics of calcium orthophosphates", Biomat. J., Vol. 31, 2010, pp. 1465-1485.
[5] Q. Fu, E. Saiz, M.N. Rahaman, A.P. Tomsia, "Bioactive glass scaffolds for bone tissue engineering: state of the art and future perspectives", Mater. Sci. Eng. C J., Vol. 31, 2011, pp. 1245-1256.
[6] Z. Gou, J. Chang, "Synthesis and in vitro bioactivity of dicalcium silicate powders", Eur. Ceram. Soc. J., Vol. 24, 2004, pp. 93-99.
[7] C. Wu, Y. Ramaswamy, H. Zreiqat, "Porous diopside ($CaMgSi_2O_6$) scaffold: A promising bioactive material for bone tissue engineering", Acta. Biomat. J., Vol. 6, 2010, pp. 2237- 3345.
[8] N. Aza, B. Zofia, M. Anseau, "Bioactivity of diopside ceramic in human", Biomed. Mater. Res. Part B.: Appl. Biomater. J., Vol. 73, 2005, pp. 54-60.
[9] S. Sadeghzade, R. Emadi, S. Labbaf, "Hardystonite-diopside nanocomposite scaffolds for bone tissue engineering applications", J. Mat. Chem. and Phy., Vol. 202, 2017, pp. 95-103.
[10] C. Wu, J. Chang, "A review bioactive silicate ceramics", J. of Biomed. Mat., Vol.8, 2013. pp.1-12.
[11] A. Najafinezhad, M. Abdellahi, H. Ghayour, A. Soheily, A. Chami, A. Khandan, "A comparative study on the synthesis mechanism, bioactivity and mechanical properties of three silicate bioceramics", J. Mat. Sci. Eng. C, Vol.72,2017, pp.259-267.
[12] S. Thomas, P. Balakrishnan, M.S. Sreekala,"Fundamental Biomaterials Ceramics", Woodhead Publishing Series in Biomaterials, 2018.
[13] C. Wu, J. Chang, "Degaradation bioactivity, and cytocompatibility of diopside, akermanite, and bredigite ceramics", Biomed. Mat. Res. Part B: Appl. Biomat. J., Vol.83, 2007, pp. 60-153.
[14] C. Wu, J. Chang, J. Wang, S. Ni, W. Zhai, "Preparation and characteristics of a calcium magnesium silicate (bredigite) bioactive ceramic", Biomat. J., Vol. 26, 2005, pp. 2925-2931.
[15] J.F. Shackelford, R.H.H. Doremus, Handbook ceramic and materials structure, properties and processing, Springer, 2008.
[16] L.H. Long, L.D. Chen, J. Chang, "Low temperature fabrication and characterizaition of β–$CaSiO_3$ ceramics", Ceram. Int. J., Vol. 32, 2006, pp. 457-460.
[17] P. Palmero, "Structural ceramic nanocomposites, a review of properties and powders synthesis methods", J. Nanomat., Vol.5, 2015 pp.656-696.
[18] F. Tavangarian, R. Emadi, "Mechanical activation assisted synthesis of pure nanocrystalline forsterite powder", J. Alloy and Compounds., Vol.485, 2009, pp.648-652.
[19] H. Ghomi, R. Emadi, S. Haghjooyeh Javamard, "Preparation of nanostructure bioactive diopside scaffolds for bone tissue engineering by two near net shape manufacturing techniques", Mat. Lett. J., Vol. 167, 2016, pp. 157-160.
[20] A. Monshi, M. Foroughi, M. Monshi, "Modifid Scherrer Equation to Estimate More Accurately Nano – Crystallite Size Using XRD", Nano. Sci. and Eng. J., Vol. 2, 2012, pp. 154-160.
[21] T. Kokubo, H.Takadama, "How useful is SBF in predicting in vivo bone bioactivity?", Biomat. J., Vol. 27, 2006, pp. 2907-2915.
[22] L. Lu, M.O. Lai, Mechanical Alloying, Kluwer Academic Publisher, Boston, 1998.
[23] G.K. Williamson, W.H. Hall, "X – ray line broadening from filed aluminum and wolfram", Acta. Metall. J., Vol. 1, 1953, pp. 22-31.
[24] C. Wu, J. Chang, "A review bioactive silicate ceramics", Biomed. Mat. J., Vol.8, 2013, pp.1-12.
[25] K. Khoshroo, T.S. Jafarzadeh, F. Moztarzadeh, M. Tahriri, H. Jazayeri, L. Tayebi, "Development of 3D PCL microsphere/TiO_2 nanotube composite scaffolds for bone tissue engineering", Mat. Sci. and Eng. C J., Vol. 70, 2017, pp.586-598